# Extremely correlated Fermi liquid study of the $U = \infty$ Anderson impurity model

B. Sriram Shastry and Edward Perepelitsky
*Physics Department, University of California, Santa Cruz, California 95064, USA*

Alex C. Hewson
*Department of Mathematics, Imperial College, 180 Queen's Gate, London, SW7 2BZ, United Kingdom*
(Received 12 July 2013; published 12 November 2013)

We apply the recently developed *extremely correlated Fermi liquid* (ECFL) theory to the Anderson impurity model, in the extreme correlation limit $U \to \infty$. We develop an expansion in a parameter $\lambda$, related to $n_d$, the average occupation of the localized orbital, and find analytic expressions for the Green's functions to $O(\lambda^2)$. These yield the impurity spectral function and also the self-energy $\Sigma(\omega)$ in terms of the two self-energies of the ECFL formalism. The imaginary parts of the latter have roughly symmetric low-energy behavior ($\propto\omega^2$), as predicted by Fermi liquid theory. However, the inferred impurity self-energy $\Sigma''(\omega)$ develops asymmetric corrections near $n_d \to 1$, leading in turn to a strongly asymmetric impurity spectral function with a skew towards the occupied states. Within this approximation, the Friedel sum rule is satisfied but we overestimate the quasiparticle weight $z$ relative to the known exact results, resulting in an overbroadening of the Kondo peak. Upon scaling the frequency by the quasiparticle weight $z$, the spectrum is found to be in reasonable agreement with numerical renormalization group results over a wide range of densities.

DOI: 10.1103/PhysRevB.88.205108 PACS number(s): 71.10.Fd, 75.30.Mb, 71.28.+d

## I. INTRODUCTION AND MOTIVATION

The *extremely correlated Fermi liquid* (ECFL) theory has been recently developed to understand the physics of correlations in the limit of infinite $U$ and applied to the $t$-$J$ model in Refs. 1 and 2. Here, we apply the ECFL theory to the problem of the spin-$\frac{1}{2}$ Anderson impurity model (AIM) at $U = \infty$. The ECFL theory is based on a systematic expansion of the formally exact Schwinger equations of motion of the model for the (Gutzwiller) projected electrons in powers of a parameter $\lambda$. This parameter is argued to be related to $n$ the density of particles in the $t$-$J$ model, and in the same spirit, to $n_d$ the average impurity level occupancy in the Anderson model considered here. Thus, at low enough densities of particles, the complete description of the system, including its dynamics, is expected in *quantitative* terms, with just a few terms in the $\lambda$ expansion. Presently, the theory to $O(\lambda^2)$ has been evaluated for the $t$-$J$ model,[2] and higher-order calculations in $\lambda$ valid up to higher densities could be carried out in principle. We thus envisage systematically cranking up the density from the dilute limit, until we hit singularities arising from phase transitions near $n \sim 1$.[3] This represents a possible road map for solving one of the hard problems of condensed matter physics and is exciting for that reason.

We apply the ECFL theory equations to $O(\lambda^2)$ to the AIM model in this work. This problem was introduced by Anderson[4] in 1961, and has been a fertile ground where several fruitful ideas and powerful techniques have been developed, and tested against experiments in Kondo, mixed valency, and heavy-fermion systems. These include the renormalization group ideas, from the intuitive poor man's scaling of Anderson[5,6] to the powerful numerical renormalization group (NRG) of Wilson,[7] Krishna-murthy *et al.*,[8] and more recent work in Refs. 9 and 10. A comprehensive review of the AIM and many popular techniques used to study it, such as the large-$N$ expansion,[11,12] slave particles,[13] and the Bethe *ansatz*,[14] can be found in Ref. 15. In the AIM, the Wilson renormalization group method provides an essentially exact solution of the crossover from weak to strong coupling, without any intervening singularity in the coupling constant. As emphasized in Refs. 16–18, the ground state is asymptotically a Fermi liquid at all densities. This implies that as a function of the density $n_d$ (at any $U$), the Fermi liquid ground state evolves smoothly without encountering any singularity, from the low-density limit (the empty orbital limit) to the intermediate-density limit (the mixed valent regime), and finally through to the very high-density limit (Kondo regime). In view of the nonsingular evolution in density, the AIM provides us with an ideal problem to benchmark the basic ECFL ideas discussed above.

The current understanding of the AIM model from Refs. 8, 16, and 17 is that Fermi liquid ground state and its attendant excitation spectrum are reached in the asymptotic sense, i.e., at low enough energies and $T$. Our present study of this model is somewhat broader. We wish to understand the excitations of the model in an enlarged region, in order to additionally obtain an estimate of the magnitude of corrections to the asymptotic behavior. To motivate this remark, note that the ECFL formalism yields an asymmetry in the excitations and the spectral functions of the $t$-$J$ model for sufficiently high densities, with a pronounced skew towards $\omega < 0$, arising fundamentally from Gutzwiller projection. This skew can be interpreted as an asymmetric correction to the leading particle-hole-symmetric excitation spectrum of that model[19] [e.g., corrections to $\Sigma''(\omega) \sim \{\omega^2 + (\pi k_B T)^2\}$ behavior of the Fermi liquid of the form $\Sigma''(\omega) \sim \omega^3$]. Such corrections have been argued to be of central importance in explaining the anomalous line shapes in the angle-resolved photoemission spectra of high-$T_c$ superconductors in the normal state.[19,20] Therefore, it is useful and important to understand the line shape and self-energy asymmetry in controlled calculations of the Anderson model with infinite $U$, which shares the local Gutzwiller constraint with the $t$-$J$ model on a lattice. A necessary condition for substantial asymmetry of the type

 

seen in ECFL at $U = \infty$ appears to be a large $U$, and hence is difficult to find from a perturbative expansion in $U$ of the type pioneered in Ref. 16. The study of the infinite-$U$ limit of the AIM is therefore particularly interesting in the present context. AIM studies of the spectral functions[21–24] using NRG have become available in recent years. We will compare our results with some of these calculations later in this paper.

In this paper, we use the ECFL machinery[2] to obtain the exact Schwinger equation of motion for the $d$-electron Green's function and represent it in terms of two self-energies. These are further expanded in a series in the parameter $\lambda$ mentioned above, and the equations to second order are arrived at. These involve a second chemical potential $u_0$ that contributes to a shift in the location of the localized energy level, bringing it closer to the chemical potential of the conduction electrons. The rationale for introducing this second chemical potential is similar to that in the $t$-$J$ model; the AIM possesses a shift invariance identified in Eq. (11). Maintaining this invariance to different orders in $\lambda$ is possible only if we introduce $u_0$. The second-order equations are studied numerically, and the solution for the spectral function is compared with the NRG results.

Since we expect some readers to be interested in the AIM more than in the $t$-$J$ model, we provide a fairly self-contained description of the ECFL method used here for the AIM. In this spirit, let us note that a direct interpretation of the parameter $\lambda$ as a partial projector can be found from a simple calculation of the atomic limit, with the parameter $\lambda$ thrown in. Reference 2 (Appendix A1 and especially Fig. 6) explicitly shows that the double occupancy goes from its maximum to zero as $\lambda$ varies from 0 to 1. Further, it is useful to view the $\lambda$ parameter in an operator sense, by writing a partially projected ($d$-orbital) fermion operator $\hat{f}^\dagger_\sigma(\lambda) = (1 - \lambda\ f^\dagger_{\bar\sigma} f_{\bar\sigma}) f^\dagger_\sigma$ and its adjoint (here $\bar\sigma = -\sigma$). The operator $\hat{f}^\dagger_\sigma(\lambda)$ interpolates between the unprojected Fermi operator $f^\dagger_\sigma$ at $\lambda = 0$, and the Gutzwiller projected Hubbard operator $X^{\sigma 0}_i$ at $\lambda = 1$. The Hamiltonian is written in terms of $\hat{f}^\dagger_\sigma(\lambda)$, $\hat{f}_\sigma(\lambda)$, and expanding in $\lambda$ gives an effective Hamiltonian that generates the auxiliary Green's function $\mathbf{g}$ below. As explained in Ref. 2, the second (caparison) part also has an expansion in $\lambda$ that follows from the Schwinger equation and the product form Eq. (12). At the end, we set the parameter $\lambda \to 1$ in the formal equations, and only then begin the actual computations. Therefore, the primary use of the parameter $\lambda$ is to count the relative orders of the terms that are higher than quadratic in the Fermi operators.

Let us first present an overview of the formal equations; the AIM model impurity Green's function $\mathcal{G}$ is written in the presence of time- and spin-dependent potentials $\mathcal{V}$, i.e., the sources of Schwinger, and their exact Schwinger equation of motion obtained in Eqs. (3) and (5). In terms of the auxiliary Green's function $\mathbf{g}$ and the caparison function $\mu$, we introduce a convolution ansatz $\mathcal{G} = \mathbf{g} \cdot \mu$ in Eq. (12). Two types of vertices are introduced by taking the functional derivatives $\frac{\delta}{\delta \mathcal{V}}$ of $\mathbf{g}^{-1}$ and $\mu$, and in terms of these, we find exact Schwinger equations of motion for $\mathbf{g}$ and $\mu$ in Eq. (14), which are expressed in terms of the two self-energies [Eq. (15)]. The auxiliary Greens's function and the physical impurity Greens's function satisfy the number sum rules in Eqs. (19) or (23), and are then expanded in the parameter $\lambda$ discussed above. An important shift invariance of the AIM is noted in the equations of motion, and a second chemical potential $u_0$ introduced as a second Lagrange multiplier to satisfy the two sum rules. To second order $O(\lambda^2)$, explicit equations are written out in Eqs. (30)–(33). The Friedel sum rule in this scheme is written out in Eq. (43), and shown to be satisfied exactly at $T = 0$. The numerical solution of the equations is performed through a spectral representation of the variables $\mathbf{g}$, and in Eq. (50) the two self-energies are written out in terms of these. These are compared with the NRG results at the same densities and results for the spectral functions of the Green's function and the self-energy are compared in detail, both before and after scaling with $z$, the quasiparticle weight.

## II. ECFL THEORY OF ANDERSON IMPURITY MODEL

### A. Model and equations for the Green's function

We consider the Anderson impurity model in the limit $U \to \infty$ given by the following Hamiltonian:

$$H = \sum_\sigma \epsilon_d X^{\sigma\sigma} + \sum_{k\sigma} \epsilon_k n_{k\sigma} + \frac{1}{\sqrt{\Omega}} \sum_{k\sigma} (V_k X^{\sigma 0} c_{k\sigma} + V^*_k c^\dagger_{k\sigma} X^{0\sigma}), \quad (1)$$

where $\Omega$ is the box volume, and we have set the Fermi energy of the conduction electrons to zero. Here, $X^{ab} = |a\rangle\langle b|$ is the Hubbard projected electron operator with $|a\rangle$ describing the empty orbital, and the two singly occupied states $a = 0, \pm\sigma$. We study the impurity Green's function

$$\mathcal{G}_{\sigma_i\sigma_f}(\tau_i, \tau_f) = -\langle\langle X^{0\sigma_i}(\tau_i)\ X^{\sigma_f 0}(\tau_f)\rangle\rangle, \quad (2)$$

with $T_\tau$ the imaginary-time ordering symbol, the definition for an arbitrary time-dependent operator $Q$: $\langle\langle Q\rangle\rangle = \langle \mathrm{Tr} T_\tau e^{-\mathcal{A}} Q\rangle / \langle \mathrm{Tr} T_\tau e^{-\mathcal{A}}\rangle$, and with the Schwinger source term $\mathcal{A} = \int_0^\beta d\tau\, \mathcal{V}^{\sigma_1\sigma_2}(\tau) X^{\sigma_1\sigma_2}(\tau)$, involving a bosonic time-dependent potential $\mathcal{V}$. Often, we abbreviate $\mathcal{V}(\tau_i) \to \mathcal{V}_i$. As usual, this potential is set to zero at the end of the calculation. In this paper, expressions such as $\mathcal{G}(\tau_i, \tau_f)$ and $\mathcal{V}$ are understood as $2 \times 2$ matrices in spin space. We assume a constant hybridization $V_k = V_0$, and a (flat) band of half-width $D$ with constant density of states $\rho(\epsilon) = \rho_0 \theta(D - |\epsilon|)$ with $\rho_0 = \frac{1}{2D}$.

Taking the time derivative of Eq. (2), we obtain the Schwinger equation of motion (EOM)

$$\{(\partial_{\tau_i} + \epsilon_d)\mathbb{1} + \mathcal{V}_i\}\mathcal{G}(\tau_i, \tau_f) = -\delta(\tau_i - \tau_f) \times [\mathbb{1} - \gamma(\tau_i)] - \frac{1}{\sqrt{\Omega}} [\mathbb{1} - \gamma(\tau_i) + \mathcal{D}_i] \cdot \sum_k V_k\, G(k, \tau_i; \tau_f), \quad (3)$$

where $\gamma(\tau_i) = \mathcal{G}^{(k)}(\tau_i^-, \tau_i)$ following Ref. 1, Eq. (35), or more explicitly in terms of spin indices as $\gamma_{\sigma_i\sigma_f}(\tau_i) = \sigma_i\sigma_f \mathcal{G}_{\bar\sigma_f\bar\sigma_i}(\tau_i, \tau_i^+)$, and with $\bar\sigma = -\sigma$. In the following, we abbreviate $\gamma(\tau_i) \to \gamma_i$. Here, we introduced the mixed Green's function $G_{\sigma_i\sigma_f}(k, \tau_i; \tau_f) = -\langle\langle c_{k\sigma_i}(\tau_i) X^{\sigma_f 0}(\tau_f)\rangle\rangle$, and a functional derivative operator $(\mathcal{D}_i)_{\sigma_i\sigma_j} = (\sigma_i\sigma_j)\, \delta/\delta \mathcal{V}^{\bar\sigma_i\bar\sigma_j}(\tau_i)$. In the ECFL formalism,[1] Eq. (3) and similar equations are to be understood as matrix equations in spin space. Following the Schwinger technique, the higher-order Green's functions have been expressed in terms of the source

functional derivatives of the basic ones; an example illustrates this: $\sigma_i\sigma_j\langle\langle X^{\bar\sigma_i\bar\sigma_j}\,Q\rangle\rangle = (\gamma_i - \mathcal{D}_i)\langle\langle Q\rangle\rangle$. Proceeding further, we take a time derivative of the mixed Green's function to find

$$\big(\partial_{\tau_i} + \epsilon_k\big)G(k,\tau_i;\tau_f) = -\frac{1}{\sqrt{\Omega}}V_k^*\,\mathcal{G}(\tau_i,\tau_f), \tag{4}$$

so combining with Eq. (3) we find the exact EOM for the localized electron Green's function:

$$\begin{aligned}&\big\{\big(\partial_{\tau_i} + \epsilon_d\big)\mathbb{1} + \mathcal{V}_i\big\}\mathcal{G}(\tau_i,\tau_f)\\ &\quad= -\delta(\tau_i - \tau_f)(\mathbb{1} - \gamma_i)\\ &\qquad- (\mathbb{1} - \gamma_i + \mathcal{D}_i)\cdot\Delta(\tau_i - \tau_{\mathbf{j}})\cdot\ \mathcal{G}(\tau_{\mathbf{j}},\tau_f),\end{aligned} \tag{5}$$

with the convention that the time label in bold letters $\tau_{\mathbf{j}}$ is to be integrated over $\in[0,\beta]$. The conduction band enters through the usual ($\mathcal{V}$-independent) function

$$\Delta(\tau_i - \tau_j) = -\frac{\mathbb{1}}{\Omega}\sum_k |V_k|^2\big(\partial_{\tau_i} + \epsilon_k\big)^{-1}\delta(\tau_i - \tau_j), \tag{6}$$

with a Fourier transform

$$\Delta(i\omega_n) = \frac{1}{\Omega}\sum_k \frac{|V_k|^2}{i\omega_n - \epsilon_k} = V_0^2\int\frac{\rho(\epsilon)d\epsilon}{i\omega_n - \epsilon}. \tag{7}$$

We will require below its analytic continuation $i\omega_n \to \omega + i\eta$:

$$\Delta(\omega + i\eta) = \Delta_R(\omega) - i\Gamma(\omega); \tag{8}$$

$$\Gamma(\omega) = \pi V_0^2\ \rho(\omega);\quad \Delta_R(\omega) = \frac{\Gamma_0}{\pi}\ln\frac{|\omega + D|}{|\omega - D|}. \tag{9}$$

Here, $\Gamma_0 = \pi V_0^2\rho_0$. We now use the noninteracting Green's function

$$\mathbf{g}_0^{-1}(\tau_i,\tau_f) = -\big[\partial_{\tau_i} + \epsilon_d + \mathcal{V}(\tau_i)\big]\delta(\tau_i - \tau_f) - \Delta(\tau_i,\tau_f), \tag{10}$$

and rewrite the fundamental equation of motion Eq. (5) as

$$\begin{aligned}&\big\{\mathbf{g}_0^{-1}(\tau_i,\tau_{\mathbf{j}}) + (\gamma_i - \mathcal{D}_i)\cdot\Delta(\tau_i - \tau_{\mathbf{j}})\big\}\cdot\mathcal{G}(\tau_{\mathbf{j}},\tau_f)\\ &\quad= (\mathbb{1} - \gamma_i)\delta(\tau_i - \tau_f).\end{aligned} \tag{11}$$

Let us note an important *shift invariance* of Eqs. (11) and (10). If we consider a transformation $\Delta(\tau) \to \Delta(\tau) + u_t \times \delta(\tau)$ with an arbitrary $u_t$, it is possible to show that Eq. (11) is unchanged, except for a shift of $\epsilon_d$ by $-u_t$. The added term $u_t(\gamma_i - \mathcal{D}_i)\mathcal{G}(\tau_i,\tau_f)$ vanishes upon using the Pauli principle and the Gutzwiller projection applicable to operators *at the same time instant*. We use this shift invariance below to introduce a second chemical potential. In the ECFL theory, we use a product *ansatz*

$$\mathcal{G}(\tau_i,\tau_f) = \mathbf{g}(\tau_i,\tau_{\mathbf{j}})\cdot\mu(\tau_{\mathbf{j}},\tau_f), \tag{12}$$

where $\mu(\tau_i,\tau_j)$ is the caparison factor, and we use this in Eq. (11). It is useful to introduce two vertex functions $\Lambda^{\sigma_1\sigma_2}_{\sigma_3\sigma_4}(\tau_n,\tau_m;\tau_i) = -\frac{\delta}{\delta\mathcal{V}_i^{\sigma_3\sigma_4}}\mathbf{g}^{-1}_{\sigma_1\sigma_2}(\tau_n,\tau_m)$ and $\mathcal{U}^{\sigma_1\sigma_2}_{\sigma_3\sigma_4}(\tau_n,\tau_m;\tau_i) = \frac{\delta}{\delta\mathcal{V}_i^{\sigma_3\sigma_4}}\mu_{\sigma_1\sigma_2}(\tau_n,\tau_m)$ as usual, and suppressing the time indices, we note $\frac{\delta}{\delta\mathcal{V}}\cdot\mathbf{g} = \mathbf{g}\cdot\Lambda\cdot\mathbf{g}$. We now use the chain rule and Eq. (12) to write $\mathcal{D}\Delta\cdot\mathcal{G} = \mathcal{D}\Delta\cdot\mathbf{g}\cdot\mu = \xi^*\Delta\cdot\mathbf{g}\cdot\Lambda_*\cdot\mathbf{g}\cdot\mu + \xi^*\Delta\cdot\mathbf{g}\cdot\ \mathcal{U}_*$, with the matrix $\xi_{\sigma\sigma'} = \sigma\sigma'$. The $*$ symbol from Ref. 1 is illustrated in component form by an example: $\ldots\xi^*_{\sigma_a\sigma_b}\ldots\delta/\delta\mathcal{V}^* = \ldots\sigma_a\sigma_b\ldots\delta/\delta\mathcal{V}^{\bar\sigma_a\bar\sigma_b}$, or in terms of the vertex functions $\ldots\xi^*_{\sigma_a\sigma_b}\ldots\Lambda_*^{\sigma'\sigma''}\ldots = \ldots\sigma_a\sigma_b\ldots\Lambda^{\sigma'\sigma''}_{\bar\sigma_a\bar\sigma_b}\ldots$, with the upper indices of $\Lambda$ governed by the rules of the matrix multiplication. Following Ref. 1 we define the linear operator $\mathbf{L}(i,j) = \xi^*\Delta(i,\mathbf{j})\cdot\mathbf{g}(\mathbf{j},j)\cdot\frac{\delta}{\delta\mathcal{V}_i^*}$. We can now collect these definitions to rewrite $\mathcal{D}\Delta\cdot\mathcal{G} = \xi^*\Delta\cdot\mathbf{g}\cdot\Lambda_*\cdot\mathbf{g}\cdot\mu + \xi^*\Delta\cdot\mathbf{g}\cdot\ \mathcal{U}_* = \Phi\cdot\mathbf{g}\cdot\mu + \Psi$, and define the two self-energies:

$$\begin{aligned}&\Phi(i,j) = -\mathbf{L}(i,\mathbf{r})\cdot\mathbf{g}^{-1}(\mathbf{r},j) = \xi^*\Delta(i,\mathbf{j})\cdot\mathbf{g}(\mathbf{j},\mathbf{k})\cdot\Lambda_*(\mathbf{k},j;i);\\ &\Psi(i,j) = \mathbf{L}(i,\mathbf{r})\cdot\mu(\mathbf{r},j) = \xi^*\Delta(i,\mathbf{j})\cdot\mathbf{g}(\mathbf{j},\mathbf{k})\cdot\ \mathcal{U}_*(\mathbf{k},j;i).\end{aligned} \tag{13}$$

Summarizing, we may rewrite the exact EOM Eq. (11) symbolically:

$$\big\{\mathbf{g}_0^{-1} + \gamma\Delta - \Phi\big\}\cdot\mathbf{g}\cdot\mu = (\mathbb{1} - \gamma)\delta + \Psi. \tag{14}$$

This equation is split into two parts by requiring $\mathbf{g}$ to be canonical:

$$\mathbf{g}^{-1} = \big\{\mathbf{g}_0^{-1} + \gamma\Delta - \Phi\big\}\quad\text{and}\quad\mu = (\mathbb{1} - \gamma)\delta + \Psi, \tag{15}$$

bringing it into the standard form in the ECFL theory.[1] Using Eq. (13), we note that the formal solutions of Eq. (15) are $\mathbf{g}^{-1} = (\mathbb{1} - \mathbf{L})^{-1}\cdot(\mathbf{g}_0^{-1} + \gamma\Delta)$ and $\mu = (\mathbb{1} - \mathbf{L})^{-1}\cdot(\mathbb{1} - \gamma)\delta$. We introduce the resolvent kernel $\mathcal{L}$ using the identity $(\mathbb{1} - \mathbf{L})^{-1} = \mathbb{1} + \mathcal{L}$ where $\mathcal{L} = (\mathbb{1} - \mathbf{L})^{-1}\cdot\mathbf{L}$. In terms of the resolvent, we see that

$$\Phi = \mathcal{L}\cdot\big(-\mathbf{g}_0^{-1} - \gamma\Delta\big)\quad\text{and}\quad\Psi = -\mathcal{L}\cdot\gamma\delta. \tag{16}$$

Therefore, distributing the action of $\mathcal{L}$ over the two terms, we can rewrite

$$\Phi = \chi + \Psi\Delta, \tag{17}$$

with

$$\chi = \mathcal{L}\cdot\big(-\mathbf{g}_0^{-1}\big). \tag{18}$$

Therefore, the self-energy $\Phi$ breaks up into two parts, as in Eq. (17). Note that in Eq. (16), the expressions $\gamma\Delta$ and $\gamma\delta$ involve multiplication at equal times, whereas in Eq. (17), $\Psi\Delta$ implies a convolution in time. The two Green's functions satisfy the pair of sum rules

$$\mathbf{g}(\tau,\tau^+) = \frac{n_d}{2};\quad\mathcal{G}(\tau,\tau^+) = \frac{n_d}{2}, \tag{19}$$

where $n_d$ is the number of electrons on the $d$ orbital $n_d = \sum_\sigma\langle X^{\sigma\sigma}\rangle$.

In the context of the $t$-$J$ model in Ref. 2, the sum rule for $\mathbf{g}$ is necessary to satisfy the Luttinger-Ward theorem. If we use the representation $\hat f^\dagger_\sigma(\lambda) = (1 - \lambda f^\dagger_{\bar\sigma}f_{\bar\sigma})f^\dagger_\sigma$ for the correlated electrons, this constraint is understandable as the constraint on the number of "uncorrelated" fermions $\langle f^\dagger_\sigma f_\sigma\rangle$, which must agree with the number of physical (correlated) electrons $\langle\hat f^\dagger_\sigma\hat f_\sigma\rangle$. Similarly, in the present case, this constraint is needed to fulfill the Friedel sum rule. We also remark that the self-energy $\Psi$, unlike its counterpart $\Phi$, is dimensionless, and thus interpreted as an adaptive spectral weight.[2]

### B. Zero source limit

Upon turning off the sources, all objects become functions of only $\tau_i - \tau_f$ and may therefore be Fourier transformed to Matsubara frequency space. By Fourier transforming

Eqs. (12), (15), and (17) and using $\gamma \to \frac{n_d}{2}$ we obtain the following expressions in frequency space:

$$\begin{aligned} \mathcal{G}(i\omega_n) &= \mathbf{g}(i\omega_n)\cdot\mu(i\omega_n), \\ \mu(i\omega_n) &= 1 - \frac{n_d}{2} + \Psi(i\omega_n), \\ \mathbf{g}^{-1}(i\omega_n) &= i\omega_n - \epsilon_d - \Delta(i\omega_n)\mu(i\omega_n) - \chi(i\omega_n). \end{aligned} \tag{20}$$

Alternately, this result can be rewritten in terms of the Dyson-Mori self-energy representation as

$$\mathcal{G}(i\omega_n) = \frac{1-\frac{n_d}{2}}{i\omega_n - \epsilon_d - \left(1-\frac{n_d}{2}\right)\Delta(i\omega_n) - \Sigma_{\rm DM}(i\omega_n)} \tag{21}$$

and

$$\begin{aligned} &\Sigma_{\rm DM}(i\omega_n) + \epsilon_d - i\omega_n \\ &\quad = \frac{1-\frac{n_d}{2}}{1-\frac{n_d}{2}+\Psi(i\omega_n)}\left[\chi(i\omega_n) + \epsilon_d - i\omega_n\right]. \end{aligned} \tag{22}$$

The sum rules (19) are

$$\sum_{i\omega_n} \mathcal{G}(i\omega_n)e^{i\omega_n\eta} = \frac{n_d}{2}; \quad \sum_{i\omega_n} \mathbf{g}(i\omega_n)e^{i\omega_n\eta} = \frac{n_d}{2}. \tag{23}$$

These are satisfied at a fixed $n_d$ using two Lagrange multipliers: the localized state energy $\epsilon_d$ and the second chemical potential $u_0$ introduced in Eq. (25). We observe that the usual Dysonian self-energy $\Sigma_{\rm AM}(i\omega_n)$ defined through the usual Dyson equation (valid for finite $U$) $G^{-1} = i\omega_n - \epsilon_d - \Delta(i\omega_n) - \Sigma_{\rm AM}(i\omega_n)$ in the infinite-$U$ limit can be obtained from

$$\Sigma_{\rm AM}(i\omega_n) = \frac{2}{2-n_d}\Sigma_{\rm DM}(i\omega_n) + \frac{n_d}{2-n_d}(\epsilon_d - i\omega_n). \tag{24}$$

The unlimited growth with $\omega_n$ makes this self-energy somewhat inconvenient to deal with, and therefore motivated the introduction of the Dyson-Mori object, which is better behaved in this regard. After analytic continuation $i\omega_n \to \omega + i0^+$, the imaginary part of $\Sigma_{\rm AM}$ is well behaved and finite as $\omega \to \infty$. It is obtained from the NRG method and compared with the relevant ECFL functions after scaling by $1 - \frac{n_d}{2}$ as in Eq. (24). We notice that the density $n_d$ appears explicitly in the expressions for the Green's functions, and must therefore be calculated self-consistently from Eq. (23). This feature is quite natural in the present approach since Eq. (3) for the Green's function contains $\gamma$ and therefore $n_d$ explicitly.

### C. Introducing λ and $u_0$ into the equations

Summarizing the work so far: Eqs. (15)–(17) follow from Eq. (11) upon using the product ansatz (12), and are exact equations. In order to get concrete results, we proceed by introducing two parameters into the equations. (i) The parameter $\lambda \in [0,1]$ multiplies certain terms shown in Eq. (25), allowing a density-type expansion, and continuously connects the uncorrelated Fermi system $\lambda = 0$ to the extremely correlated case $\lambda = 1$. (ii) The second parameter $u_0$ is introduced as shown in Eq. (25). It is the second chemical potential used to enforce the shift identities of the exact equation (11). Equation (11) now becomes

$$\left\{\mathbf{g}_0^{-1} + \lambda(\gamma - \mathcal{D})\left(\Delta - \frac{u_0}{2}\delta\right)\right\}\cdot\mathcal{G} = (\mathbb{1} - \lambda\gamma)\delta. \tag{25}$$

As a consequence, in Eq. (14) to Eq. (18) we set $\gamma \to \lambda\gamma$, $\Psi \to \lambda\Psi$, and $\Phi \to \lambda\Phi$, or $\chi \to \lambda\chi$. Second, in Eq. (14) to Eq. (18) we set $\Delta(\tau_i,\tau_f) \to \Delta(\tau_i,\tau_f) - \frac{u_0}{2}\,\delta(\tau_i - \tau_f)$. Note that there is no shift of Eq. (10) implied in Eq. (25).

We write Eq. (15) with λ inserted explicitly and the understanding that $\Delta(\tau_i,\tau_f)$ has been shifted as[25]

$$\begin{aligned} \mathbf{g}^{-1}(\tau_i,\tau_f) &= \mathbf{g}_0^{-1}(\tau_i,\tau_f) + \lambda\gamma(\tau_i)\Delta(\tau_i,\tau_f) - \lambda\,\Phi(\tau_i,\tau_f), \\ \mu(\tau_i,\tau_f) &= \delta(\tau_i - \tau_f)[\mathbb{1} - \lambda\gamma(\tau_i)] + \lambda\,\Psi(\tau_i,\tau_f), \end{aligned} \tag{26}$$

where the two self-energies are given in terms of the vertex functions as

$$\begin{aligned} \Phi(\tau_i,\tau_f) &= \xi^*\Delta(\tau_i,\tau_{\mathbf{j}})\cdot\mathbf{g}(\tau_{\mathbf{j}},\tau_{\mathbf{k}})\cdot\Lambda_*(\tau_{\mathbf{k}},\tau_f;\tau_i), \\ \Psi(\tau_i,\tau_f) &= \xi^*\Delta(\tau_i,\tau_{\mathbf{j}})\cdot\mathbf{g}(\tau_{\mathbf{j}},\tau_{\mathbf{k}})\cdot\mathcal{U}_*(\tau_{\mathbf{k}},\tau_f;\tau_i). \end{aligned} \tag{27}$$

On switching off the sources, these expressions can be spin resolved and expressed as $\Phi = \Delta\mathbf{g}\Lambda^{(a)}$ and $\Psi = \Delta\mathbf{g}\,\mathcal{U}^{(a)}$, with the same time labels as above, and with the usual spin decomposition $\Lambda^{(a)} = \Lambda^{\sigma\sigma}_{\bar\sigma\bar\sigma} - \Lambda^{\sigma\bar\sigma}_{\sigma\bar\sigma}$.

### D. λ expansion

We note that we can obtain the equations of motion for the Anderson model from the equations of motion for the $t$-$J$ model by making the following substitutions and replacing all space-time variables with just time[26]:

$$\begin{aligned} t[i,f] \to -\Delta(\tau_i,\tau_f); \quad \varepsilon_k \to \Delta(i\omega_k), \\ J \to 0, \quad \boldsymbol{\mu} \to -\epsilon_d. \end{aligned} \tag{28}$$

The λ expansion for the Anderson model is therefore analogous to the one for the $t$-$J$ model in Ref. 2 and the large-$d$ $t$-$J$ model in Ref. 26, and can be obtained from them by making the substitutions in Eq. (28) and changing all frequency momentum four-vectors to just frequency. For completeness, Appendix A provides a brief derivation (in time domain) of the following equations. Denoting

$$a_{\mathcal{G}} = 1 - \lambda\frac{n_d}{2} + \lambda^2\frac{n_d^2}{4}, \tag{29}$$

and the frequently occurring object

$$\mathcal{R} = \mathbf{g}(i\omega_p)\mathbf{g}(i\omega_q)\mathbf{g}(i\omega_p + i\omega_q - i\omega_n),$$

we obtain to $O(\lambda^2)$ the expressions

$$\mathcal{G}(i\omega_n) = \mathbf{g}(i\omega_n)\mu(i\omega_n), \quad \mu(i\omega_n) = a_{\mathcal{G}} + \lambda\Psi(i\omega_n), \tag{30}$$

$$\mathbf{g}^{-1}(i\omega_n) = i\omega_n - \epsilon_d' - \left(\Delta(i\omega_n) - \frac{u_0}{2}\right)\mu(i\omega_n) - \lambda\chi(i\omega_n), \tag{31}$$

$$\begin{aligned} \chi(i\omega_n) = -\lambda\sum_{p,q}&[2\Delta(i\omega_p) - u_0] \\ &\times\left[\Delta(i\omega_p + i\omega_q - i\omega_n) - \frac{u_0}{2}\right]\mathcal{R}, \end{aligned} \tag{32}$$

$$\Psi(i\omega_n) = -\lambda\sum_{p,q}[2\Delta(i\omega_p) - u_0]\mathcal{R}. \tag{33}$$

The energy $\epsilon_d'$ is given by collecting the static terms in $\Phi$ as

$$\epsilon_d' = \epsilon_d + u_0\left(\lambda\frac{n_d}{2} - \lambda^2\frac{n_d^2}{8}\right) + \frac{u_0}{2}a_{\mathcal{G}} - \lambda\sum_{i\omega_p}\Delta(i\omega_p)\mathbf{g}(i\omega_p). \quad (34)$$

The shift theorem is satisfied by all the terms separately since we have taken care to form expressions of the type $\Delta - \frac{u_0}{2}$. As discussed in Ref. 2, the shift theorems mandate the introduction of $u_0$, and its availability, in addition to $\epsilon_d$, enables us to fix the pair of sum rules (19). As explained, we must set $\lambda \to 1$ before using these expressions.

Within the $O(\lambda^2)$ theory, the total spectral weight of the Green's function is $a_{\mathcal{G}}$ rather than the exact value $1 - \frac{n_d}{2}$. This is understood as the incomplete projection to single occupancy leading to an excess in the total number of states available to the system. In order to ensure that $\Sigma_{\rm DM}(\omega)$ retain the feature of being finite as $\omega \to \infty$, it must be slightly redefined (to $\hat{\Sigma}_{\rm DM}$) in the $O(\lambda^2)$ theory:

$$G(\omega) = \frac{a_{\mathcal{G}}}{\omega - \epsilon_d'' - a_{\mathcal{G}}\Delta(\omega) - \hat{\Sigma}_{\rm DM}(\omega)}, \quad (35)$$

where

$$\epsilon_d'' \equiv \epsilon_d' - \frac{u_0}{2}a_{\mathcal{G}}. \quad (36)$$

Using Eqs. (30) and (31), we can relate $\hat{\Sigma}_{\rm DM}(\omega)$ to $\chi(\omega)$ and $\Psi(\omega)$:

$$\hat{\Sigma}_{\rm DM}(\omega) + \epsilon_d' - \omega = \frac{a_{\mathcal{G}}}{a_{\mathcal{G}} + \Psi(\omega)}[\chi(\omega) + \epsilon_d' - \omega]. \quad (37)$$

Since $\Psi(\omega),\chi(\omega) \to 0$ as $\omega \to \infty$, we see explicitly that $\hat{\Sigma}_{\rm DM}(\omega)$ remains finite in this limit. Just as in the case of Im $\Sigma_{\rm DM}(\omega)$, Im $\hat{\Sigma}_{\rm DM}(\omega)$ is related to Im $\Sigma_{\rm AM}(\omega)$ by a multiplicative constant ($1 - \frac{n_d}{2}$ and $a_{\mathcal{G}}$, respectively), and therefore their spectra are identical apart from this multiplicative constant. Comparing Eqs. (21) and (35), we see that the latter is obtained from the former with the substitutions

$$\Sigma_{\rm DM}(\omega) \to \hat{\Sigma}_{\rm DM}(\omega); \quad \epsilon_d \to \epsilon_d''; \quad 1 - \frac{n_d}{2} \to a_{\mathcal{G}}. \quad (38)$$

Keeping these substitutions in mind, we will now only use $\Sigma_{\rm DM}(\omega)$ from the exact theory, with the understanding that the same expressions hold for $\hat{\Sigma}_{\rm DM}(\omega)$ in the $O(\lambda^2)$ theory as long as the substitutions in Eq. (38) are made.

### E. Friedel sum rule at $T = 0$

At $T = 0$, the Friedel sum rule[27–29] plays an important role in the AIM, parallel to that of the Luttinger-Ward volume theorem in Fermi liquids. In Ref. 29, the original form of the Friedel sum rule is written in terms of $\eta_\sigma(\omega)$, the phase shift of the conduction electron with spin $\sigma$ at energy $\omega$:

$$\eta_\sigma(\omega) = \frac{1}{2i}\ln\left[\mathcal{G}_\sigma(\omega + i0^+)\mathcal{G}_\sigma^{-1}(\omega - i0^+)\right], \quad (39)$$

where the logarithm is chosen with a branch cut along the positive real axis, so that $0 \leqslant \eta \leqslant \pi$. The Friedel sum rule is then written as

$$\eta_\sigma(\omega = 0) = \frac{\pi n_d}{2}. \quad (40)$$

This theorem is proven for the AIM at finite $U$ (Ref. 29) by adapting the argument of Luttinger and Ward[30] with an implicit assumption of a nonsingular evolution in $U$ from 0. We assume that the Friedel sum rule also holds in the extreme correlation limit $U \to \infty$. Using the Dyson-Mori representation (21) to compute the phase shift in Eq. (39), we may rewrite this as

$$n_d = 1 - \frac{2}{\pi}\tan^{-1}\left[\frac{\epsilon_d + \text{Re }\Sigma_{\rm DM}(0)}{\Gamma_0\left(1 - \frac{n_d}{2}\right)}\right], \quad (41)$$

with $\epsilon_d + \text{Re }\Sigma_{\rm DM}(0) > 0$, in the physical case of $0 \leqslant n_d \leqslant 1$. It is easily seen[32] that this form is equivalent to the standard statement of the Friedel sum rule[15]

$$\rho_{\mathcal{G}}(0) = \frac{1}{\pi\Gamma_0}\sin^2\left(\frac{\pi n_d}{2}\right). \quad (42)$$

Within the approximation of the $\lambda$ expansion, the Friedel sum rule implies a relationship between the values of the two self-energies at zero frequency:

$$n_d = 1 - \frac{2}{\pi}\tan^{-1}\left[\frac{\epsilon_d' - \frac{u_0}{2}\mu(0) + \chi(0)}{\Gamma_0\mu(0)}\right]. \quad (43)$$

This can be obtained by using the substitutions from Eq. (38) in Eq. (41), and using Eqs. (37), (36), and (30).

We can also record a result for the auxiliary density of states $\rho_{\mathbf{g}}(\omega = 0)$, analogous to Eq. (42) here. It follows from Eq. (47), with the Fermi liquid type assumption of vanishing of $\rho_\Psi(0)$ at $T = 0$, and reads as

$$\rho_{\mathbf{g}}(0) = \frac{1}{\pi\Gamma_0\mu(0)}\sin^2\left(\frac{\pi n_d}{2}\right). \quad (44)$$

We check the validity of the Friedel sum rule within the $\lambda$ expansion in both the forms (42) and (43). In doing so, we are thus testing if the strategy of the two ECFL sum rules [Eq. (23)] enforces the Friedel sum rule, in a situation that is essentially different from that in finite-$U$ theories so that the central result of Luttinger and Ward[30] is not applicable in any obvious way.

### F. Computation of spectral function

In computing the spectral function, we follow the approach taken in Ref. 2, in which the spectral function is calculated for the $O(\lambda^2)$ ECFL theory of the $t$-$J$ model. Our calculation is made simpler due to the absence of any spatial degrees of freedom, but more complicated by the presence of the frequency-dependent factor $\Delta(i\omega_n)$. We define the various spectral functions and the relationships between them. These expressions are analogous to those in Sec. III A of Ref. 2:

$$Q(i\omega_n) = \int_{-\infty}^{\infty} d\nu \frac{\rho_Q(\nu)}{i\omega_n - \nu}, \quad (45)$$

where $Q$ can stand for any object such as $\mathcal{G}$, $\mathbf{g}$, $\chi$, $\Sigma_{\rm DM}$, or $\Psi$. Therefore, after analytic continuation $i\omega_n \to \omega + i0^+$,

$$\rho_Q(\omega) \equiv -\frac{\text{Im}}{\pi}Q(\omega + i0^+) \quad \text{and} \quad \text{Re }Q(\omega) = \mathcal{H}[\rho_Q](\omega), \quad (46)$$

where for any real density $\rho_Q(\omega)$ the Hilbert transform is denoted as $\mathcal{H}[\rho_Q](\omega) = P\int_{-\infty}^{\infty} d\nu \frac{\rho_Q(\nu)}{\omega - \nu}$. From Eq. (33), we

TABLE I. The bare impurity level $\epsilon_d$ as well as the quasiparticle weight $z$ are displayed for the ECFL and the NRG calculations for all values of the density. Additionally, the theoretical value for the Friedel sum rule as well as the ECFL deviation from it are displayed.

| $n_d$ | $\rho_{G,\mathrm{ECFL}}(0)$ | $\epsilon_{d,\mathrm{ECFL}}$ | $\epsilon_{d,\mathrm{NRG}}$ | $z_{\mathrm{ECFL}}$ | $z_{\mathrm{NRG}}$ |
|---|---|---|---|---|---|
| 0.35 | 8.69 + 1.8% | −0.003 | −0.003 | 0.753 | 0.697 |
| 0.441 | 13.0 + 1.1% | −0.010 | −0.009 | 0.661 | 0.567 |
| 0.536 | 17.7 + 0.73% | −0.015 | −0.015 | 0.559 | 0.416 |
| 0.6 | 20.8 + 0.41% | −0.019 | −0.018 | 0.489 | 0.312 |
| 0.7 | 25.3 + 0.62% | −0.024 | −0.024 | 0.388 | 0.169 |
| 0.777 | 28.1 + 0.26% | −0.031 | −0.029 | 0.314 | 0.081 |
| 0.834 | 29.7 + 0.20 % | −0.037 | −0.035 | 0.265 | 0.035 |

find that

$$\rho_{\mathcal{G}}(\omega) = \rho_{\mathbf{g}}(\omega)[a_{\mathcal{G}} + \mathrm{Re}\,\Psi(\omega)] + \rho_{\Psi}(\omega)\mathrm{Re}\,\mathbf{g}(\omega). \quad (47)$$

With $f(\omega) = \frac{1}{1+e^{\beta\omega}}$ and $\bar{f}(\omega) = 1 - f(\omega)$, the two sum rules (23) read as

$$\int_{-\infty}^{\infty} f(\omega)\rho_{\mathbf{g}}(\omega)d\omega = \frac{n_d}{2}, \quad \int_{-\infty}^{\infty} f(\omega)\rho_{\mathcal{G}}(\omega)d\omega = \frac{n_d}{2}. \quad (48)$$

We also note $\rho_{\Delta}(\omega) = \frac{\Gamma(\omega)}{\pi}$. It is useful to define a mixed (composite) density

$$\rho_M(x) = \rho_{\mathbf{g}}(x)\left(\Delta_R(x) - \frac{u_0}{2}\right) + \rho_{\Delta}(x)\mathrm{Re}\,\mathbf{g}(x), \quad (49)$$

so that we can integrate (or sum) the internal frequencies in Eq. (33) efficiently (see Appendix B), and write the two relevant complex self-energies (with $\omega \equiv \omega + i0^+$) as

$$\Psi(\omega) = -2\lambda \int_{u,v,w} \frac{\rho_M(u)\rho_{\mathbf{g}}(v)\rho_{\mathbf{g}}(w)}{\omega - u - v + w} \times [f(u)f(v)\bar{f}(w) + \bar{f}(u)\bar{f}(v)f(w)],$$

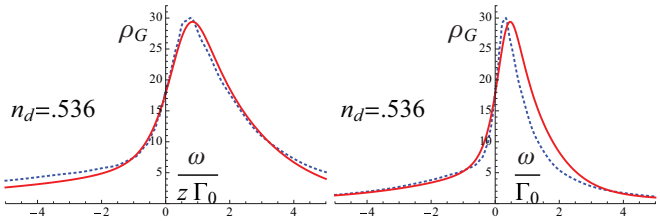


FIG. 2. (Color online) The spectral density for the physical Green's function for the density of $n_d = 0.536$. For the plot on the left, both the ECFL and NRG curves are plotted versus $\frac{\omega}{\Gamma_0 z}$. Since ECFL has a larger $z$ value, the absolute scale of the $\omega$ axis differs for the two curves. For the plot on the right, both ECFL and NRG are plotted versus $\frac{\omega}{\Gamma_0}$ and hence the ECFL peak is too wide.

$$\chi(\omega) = -2\lambda \int_{u,v,w} \frac{\rho_M(u)\rho_{\mathbf{g}}(v)\rho_M(w)}{\omega - u - v + w} \times [f(u)f(v)\bar{f}(w) + \bar{f}(u)\bar{f}(v)f(w)]. \quad (50)$$

In these expressions, $u, v, w$ are understood to be real variables, and using Eq. (46) we can extract the real and imaginary parts of $\Psi$ and $\chi$ in terms of the spectral functions.

## III. RESULTS

The following explicit results were obtained after setting $\lambda = 1$ in the equations noted above. We calculated the spectral functions $\rho_G$, $\rho_\Sigma$, $\rho_\chi$, and $\rho_\Psi$ using the values $D = 1$, $\Gamma_0 = 0.01$, and $T = 0$. The zero-temperature limit is easily achieved in the ECFL theory by setting all of the Fermi functions to step functions. We expect that the spectral function calculated within the ECFL $O(\lambda^2)$ theory will be accurate through a density of approximately $n_d = 0.6$, or perhaps at best $n_d \sim 0.7$. As discussed in Refs. 1 and 2, this is the main limitation of the low-order $\lambda$ results: the theory begins to have substantial corrections as we increase $n_d$ towards unity. The source of this error estimate is the high-frequency behavior

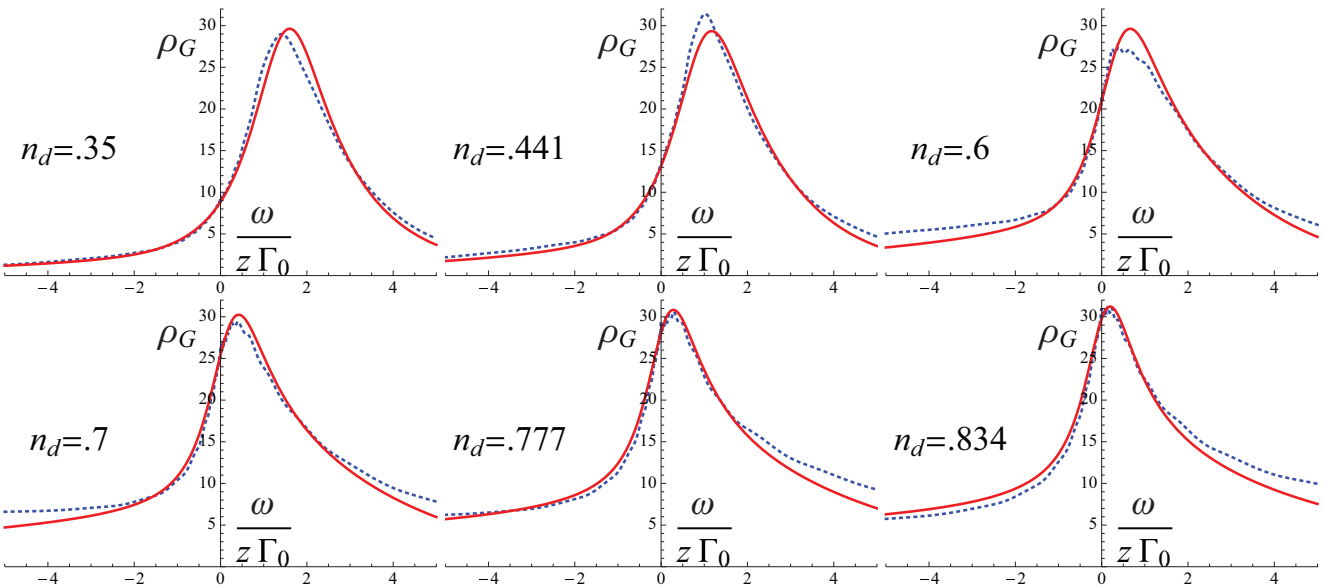


FIG. 1. (Color online) The spectral density for the physical Green's function versus $\frac{\omega}{\Gamma_0 z}$ for densities of $n_d = 0.35, 0.441, 0.6, 0.7, 0.777, 0.834$. The red curve is the ECFL calculation, while the blue curve is the NRG calculation.

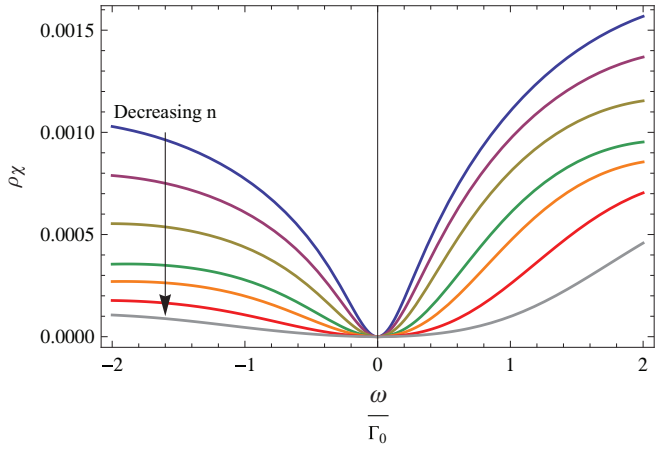


FIG. 3. (Color online) The spectral function for $\chi$ for densities of $n_d = 0.834,0.777,0.7,0.6,0.536,0.441,0.35$.

within the $\lambda$ expansion of the Green's function (33) $\mathcal{G} \sim \frac{a_G}{i\omega}$; this deviates from the known exact behavior $\mathcal{G} \sim \frac{1-n_d/2}{i\omega}$. The error grows with increasing density, but we expect to have reasonable results even at $n_d = 0.7$.

In Table I, we show the results for the spectral function at zero energy in terms of the percentage deviation from the Friedel sum rule (42), demonstrating that the ECFL satisfies the Friedel sum rule to a high degree of accuracy. We specify the occupation number $n_d$ and show the values of the energy level $\epsilon_d$ and quasiparticle weight $z$ calculated within the ECFL and NRG calculations. The values of $\epsilon_d$ are in good agreement between the two calculations, while there is a discrepancy in $z$ which becomes more pronounced at higher densities. While the error in the scale of $z$ as $n_d \to 1$ is expected from the low order in $\lambda$ aspect of the theory, we should keep in mind that the *shape* of the spectral function, and also the imaginary part of the self-energy, is another matter altogether. We display below these objects after scaling the frequency with $z$: this captures the *shape* of the spectra and isolates the discrepancy to a single number, namely, the magnitude of $z$. The admittedly nontrivial problem of the magnitude of $z$ must await a more satisfactory resolution involving the treatment of higher-order terms in $\lambda$.

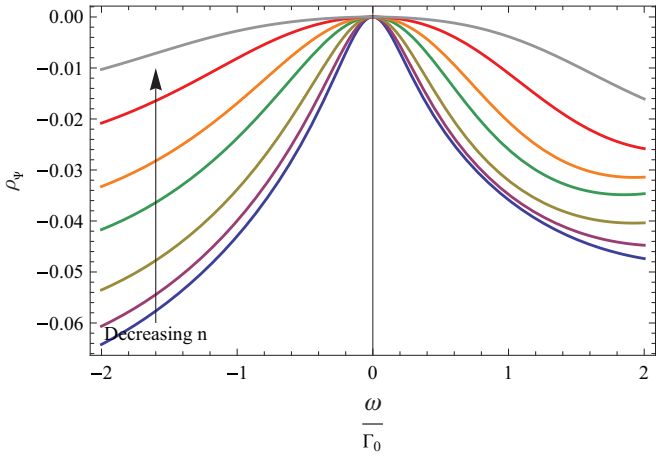


FIG. 4. (Color online) The spectral function for $\Psi$ for densities of $n_d = 0.834,0.777,0.7,0.6,0.536,0.441,0.35$.

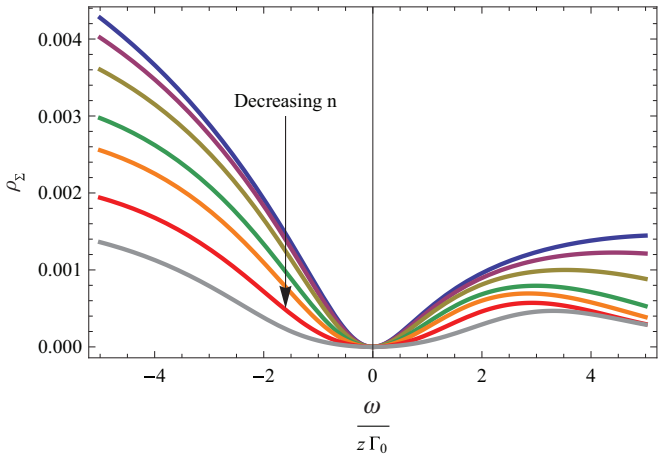


FIG. 5. (Color online) The spectral function for the Dyson-Mori self-energy for densities of $n_d = 0.834,0.777,0.7,0.6,0.536,0.441,0.35$. The curvature of the quadratic minimum becomes larger with increasing density.

In Fig. 1 we display the spectral functions at the indicated densities, indicating a smooth evolution with density. The Kondo or Abrikosov-Suhl resonance at positive frequencies becomes sharper as we increase density and moves closer to $\omega = 0$. If the raw ECFL and NRG spectral functions are compared (as in right panel of Fig. 2 for $n_d = 0.536$), one finds that the peak in the ECFL spectral function is too broad. This overbroadening becomes worse at larger densities and better at lower densities. However, it can be understood well in terms of the elevated value of $z$ for ECFL at higher densities. Hence, before doing the comparison, as in Fig. 1, we first rescale the $\omega$ axis for both the ECFL and NRG spectral functions by the appropriate $z$ (as in the left panel of Fig. 2 for $n_d = 0.536$ and in Fig. 1 for the other densities). They are then found to be in good agreement up to surprisingly high values of $n_d$, suggesting that the ECFL theory captures the *shape* (but not the scale) of the spectral functions and their asymmetry in a very natural fashion. We also found good agreement with the NRG spectral functions in Ref. 24. The ECFL spectral function $\rho_G$ is constructed out of the two spectral functions $\rho_\chi$ and $\rho_\Psi$ that are shown at various densities in Figs. 3 and 4, exhibiting Fermi liquid type quadratic frequency dependence at low $\omega$.

In Fig. 5 we present the density evolution of the spectral function for the Dyson-Mori self-energy [see Eq. (22)]. This exhibits a remarkable similarity to the analogous spectral density for the $t$-$J$ model in the limit of high dimensions[33] and the Hubbard model at large $U$.[34]

## IV. CONCLUSION

In this work, we have applied the ECFL formalism at the simplest level, using the $O(\lambda^2)$ equations, to the Anderson impurity model with $U \to \infty$. In this formalism, the two self-energies of the ECFL theory $\Psi$ and $\chi$ are calculated using a skeleton expansion in the auxiliary Green's function $\mathbf{g}$. This is analogous to the skeleton expansion for the Dyson self-energy $\Sigma$, in standard Feynman-Dyson perturbation theory applicable to the case of finite $U$. These two self-energies determine $\mathbf{g}$ as well as the physical $\mathcal{G}$, leading to a self-consistent solution. We

obtained the equations to second order and solved them numerically at $T = 0$. We found that at low enough $\omega$, the ECFL self-energies have symmetric spectra of the type predicted by Fermi liquid theory (see Figs. 3 and 4). Combining them through the ECFL functional form (22) generates a nontrivial self-energy with an asymmetric spectrum displayed in Fig. 5. It therefore appears that functional form (22) has the potential to generate realistic and nontrivial spectral densities, starting with rather simple components. The availability of convenient and natural analytical expressions is seen to provide a distinct advantage of the ECFL formalism. Formally exact techniques such as the NRG involve steps that are not automatically endowed with these, but rather rely on analytic continuation or other equivalent techniques.

The physical spectral function for the impurity site is obtained from the above pair of ECFL self-energies, and displays a Kondo or Abrikosov-Suhl resonance. This feature becomes more narrow and the spectrum becomes more skewed towards the occupied side of the peak with increasing density. However, the computed quasiparticle $z$ in the present calculation is considerably larger than the exact value $z \propto e^{-1/2(1-n_d)}$, as $n_d \to 1$,[31] i.e. into the Kondo regime. This large $z$ makes it impossible for the $O(\lambda^2)$ version of ECFL presented here to address the Kondo regime $n_d \to 1$. It results in the the masking of a small (and broad) peak at $\omega \sim \epsilon_d$, found in our NRG spectral functions, as we approach the Kondo limit. Both real and imaginary parts of the computed $\Sigma_{\rm DM}(\omega)$ are larger than their NRG counterparts in that regime, thereby precluding a peak.

To place this result in context, we observe that the same level of approximation of ECFL, applied to the lattice problem of the $d \to \infty$, $U \to \infty$ Hubbard model in Ref. 33 (see Fig. 12), *does* show a lower Hubbard band peak in the spectral function. This difference presumably arises from the robust value of $z \sim (1-n)$ in the lattice model, arising from Gutzwiller physics; it is much larger than the exponentially small value $z \propto e^{-1/2(1-n_d)}$ in the AIM. Therefore, the fractional error made by the $O(\lambda^2)$ ECFL calculation is smaller in the lattice model compared to the AIM.

The location of the peak is set by $\epsilon_d + \Sigma_{\rm DM}(0)$ [Eq. (21)]. Using Eq. (41), we can see that this quantity must decrease with increasing density. This is consistent with the expectation that the location of the peak will approach $\omega = 0$ as $n_d \to 1$. This can also be understood from the need to have more spectral weight when $\omega \leqslant 0$, to yield a higher value of $n_d$. We found that the ECFL spectrum satisfies the Friedel sum rule [Eq. (42)] to a high degree of accuracy, and that ECFL yields values of $\epsilon_d$ in good agreement with the NRG values at all densities (see Table I).

As mentioned above, the ECFL calculation to $O(\lambda^2)$ overestimates the value of the quasiparticle weight $z$ as compared with the NRG and the exact asymptotic result $z \propto e^{-1/2(1-n_d)}$ as $n_d \to 1$,[31] the difference becoming more significant with increasing density. This also leads to an overbroadening of the peak in the ECFL spectrum at higher densities. This is consistent with the fact that the $\lambda$ expansion of the ECFL is a low-density expansion and the current calculation has only been carried out to $O(\lambda^2)$. Nevertheless, after rescaling the $\omega$ axis for both the ECFL and NRG spectra by their respective values of $z$, we find good quantitative agreement between the two as in Fig. 1. In Fig. 2, we illustrate the comparison between scaled and unscaled spectral functions at a typical density. We find similarly good agreement with the NRG calculation from Ref. 24. This implies that the ECFL theory has the correct *shape* of the spectra built into it quite naturally.

Finally, we note that the computed spectral functions exhibit a remarkable similarity to the analogous spectral density for the $t$-$J$ model in the limit of high dimensions[33] and the Hubbard model at large $U$.[34]

## ACKNOWLEDGMENTS

This work was supported by DOE under Grant No. FG02-06ER46319. We thank H. R. Krishna-murthy for helpful comments.

## APPENDIX A: CALCULATING THE SELF-ENERGIES IN THE $O(\lambda^2)$ THEORY

The calculation follows the procedure given in Ref. 2. A few comments are provided to make the connections explicit: the zeroth-order vertices are common to Ref. 2 [Eqs. (B3) and (B14)] and the first-order $\mathcal{U}$ is common to Eq. (B15). The first-order vertex $[\Lambda]_1$ can be found parallel to Eqs. (B23)–(B28) in Ref. 2 from differentiating

$$[\mathbf{g}^{-1}(i,f)]_1 = \Delta(i,f)\mathbf{g}^{(k)}(i,i) + \delta(i,f)\Delta(i,\mathbf{a})\mathbf{g}^{(k)}(\mathbf{a},f), \tag{A1}$$

as

$$[\Lambda^{(a)}(i,m;j)]_1 = -2\Delta(i,m)\mathbf{g}(i,j)\cdot\mathbf{g}(j,i) - 2\delta(i,m)\Delta(i,\mathbf{k})\mathbf{g}(\mathbf{k},j)\cdot\mathbf{g}(j,i). \tag{A2}$$

Here, the bold labels are integrated over. From this we construct, the time-domain self-energies

$$\Psi(i,f) = -2\lambda\Delta(i,\mathbf{k})\mathbf{g}(\mathbf{k},f)\cdot\mathbf{g}(i,f)\cdot\mathbf{g}(f,i) \tag{A3}$$

and

$$\Phi(i,f) = -\delta(i,f)\Delta(i\mathbf{k})\mathbf{g}(\mathbf{k}i) - 2\lambda\Delta(i\mathbf{j})\mathbf{g}(\mathbf{j}\mathbf{k})\cdot\Delta(\mathbf{k}f)\mathbf{g}(\mathbf{k}i)\cdot\mathbf{g}(i\mathbf{k}) - 2\lambda\Delta(i\mathbf{j})\mathbf{g}(\mathbf{j}f)\cdot\Delta(f\mathbf{k})\mathbf{g}(\mathbf{k}i)\cdot\mathbf{g}(if). \tag{A4}$$

After shifting $\Delta(i,f) \to \Delta(i,f) - \frac{u_0}{2}\delta(i,f)$ and Fourier transforming these, we obtain Eqs. (33) and (34). These expressions for the self-energies are correct to $O(\lambda)$ and lead to expression for $\mathbf{g}^{-1}$ and $\mu$ which are correct to $O(\lambda^2)$. $\chi$ can be extracted from $\Phi$ as indicated in the text.

## APPENDIX B: FREQUENCY SUMMATIONS

An efficient method to perform the frequency sums is to work with the time-domain formulas (A3) and (A4) until the final step where Fourier transforms are taken. We note the representation for the Green's function

$$\mathbf{g}(\tau) = \int_x \rho_{\mathbf{g}}(x)e^{-\tau x}[\theta(-\tau)f(x) - \theta(\tau)\bar{f}(x)], \tag{B1}$$

so that we can easily compound any pair that arises by dropping the cross products $\theta(\tau)\theta(-\tau)$ and using $\theta(\tau)^2 = \theta(\tau)$. An

example illustrates this procedure:

$$\mathbf{g}(\tau)\mathbf{g}(-\tau) = -\int_{x,y} \rho_{\mathbf{g}}(x)\rho_{\mathbf{g}}(y)e^{-\tau(x-y)} \times [\theta(-\tau)f(x)\bar{f}(y) + \theta(\tau)\bar{f}(x)f(y)]. \quad \text{(B2)}$$

We also need to deal with the convolution of pairs of functions

$$X(\tau) = \int_{-\beta}^{\beta} d\bar{\tau}\, \mathbf{g}(\bar{\tau})\left[\Delta(\tau-\bar{\tau}) - \frac{u_0}{2}\delta(\tau-\bar{\tau})\right] = \int_x \rho_M(x)e^{-\tau x}[\theta(-\tau)f(x) - \theta(\tau)\bar{f}(x)], \quad \text{(B3)}$$

where the density $\rho_M(x)$ is defined in Eq. (49). This equation in turn is easiest to prove by transforming into a product in the Matsubara frequency space, simplifying using partial fractions, and then transforming back to time domain. We next note that Eqs. (A3) and (A4) imply

$$\Psi(\tau) = -2\lambda X(\tau)\mathbf{g}(\tau)\mathbf{g}(-\tau), \qquad \chi(\tau) = -2\lambda X(\tau)X(-\tau)\mathbf{g}(\tau), \quad \text{(B4)}$$

so that taking Fourier transforms is simplest if we first multiply out as in Eq. (B2), leading to Eq. (50).


[1] B. S. Shastry, Phys. Rev. Lett. **107**, 056403 (2011).

[2] B. S. Shastry, Phys. Rev. B **87**, 125124 (2013); D. Hansen and B. S. Shastry, *ibid.* **87**, 245101 (2013).

[3] Aficionados will recognize this as the case for the virial expansion in statistical mechanics, where a low-density expansion can often be found for very strongly interacting systems. The critical density (where a phase transition occurs) is a natural boundary for such an expansion. If one knows *a priori* that there is no critical density in a given problem such as the Anderson model, then this expansion can be pushed to arbitrarily high densities. In the very different context of the theory of integrable systems in one dimension, this is precisely the reason why the *asymptotic Bethe ansatz* works very well, even yielding exact results in regimes where its validity seems *a priori* only approximate, as explained in Bill Sutherland, *Beautiful Models* (World Scientific, Singapore, 2004).

[4] P. W. Anderson, Phys. Rev. **124**, 41 (1961).

[5] P. W. Anderson, Phys. Rev. **164**, 352 (1967); P. W. Anderson and G. Yuval, Phys. Rev. Lett. **23**, 89 (1969).

[6] F. D. M. Haldane, Phys. Rev. Lett. **40**, 416 (1978).

[7] K. G. Wilson, Rev. Mod. Phys. **47**, 773 (1975).

[8] H. R. Krishna-murthy, J. W. Wilkins, and K. G. Wilson, Phys. Rev. B **21**, 1044 (1980).

[9] A. C. Hewson, A. Oguri, and D. Meyer, Eur. Phys. J. B **40**, 177 (2004); K. Edwards, A. C. Hewson, and V. Pandis, Phys. Rev. B **87**, 165128 (2013).

[10] D. E. Logan, M. P. Eastwood, and M. A. Tusch, J. Phys. Condens. Matter **10**, 2673 (1998); M. T. Glossop and D. E. Logan, *ibid.* **14**, 6737 (2002).

[11] N. Bickers, Rev. Mod. Phys. **59**, 845 (1987).

[12] N. Read and D. M. Newns, J. Phys. C: Solid State Phys. **16**, L1055 (1983); N. Read, *ibid.* **18**, 2651 (1985).

[13] P. Coleman, Phys. Rev. B **29**, 3035 (1984); S. E. Barnes, J. Phys. F: Met. Phys. **6**, 1375 (1976).

[14] N. Andrei, Phys. Rev. Lett. **45**, 379 (1980); P. B. Wiegmann, Sov. Phys.–JETP **31**, 392 (1980).

[15] A. C. Hewson, *The Kondo Problem to Heavy Fermions* (Cambridge University Press, Cambridge, UK, 1993).

[16] K. Yosida and K. Yamada, Prog. Theor. Phys. Suppl. **46**, 244 (1970).

[17] P. Nozières, J. Low. Temp. Phys. **17**, 31 (1974).

[18] A. C. Hewson, Phys. Rev. Lett. **70**, 4007 (1993).

[19] B. S. Shastry, Phys. Rev. Lett. **109**, 067004 (2012).

[20] G.-H. Gweon, B. S. Shastry, and G. D. Gu, Phys. Rev. Lett. **107**, 056404 (2011).

[21] H. O. Frota and L. N. Oliveira, Phys. Rev. B **33**, 7871 (1986).

[22] O. Sakai, Y. Shimuzu, and T. Kasuya, J. Phys. Soc. Jpn. **58**, 162 (1989).

[23] T. A. Costi and A. C. Hewson, J. Phys.: Condens. Matter **5**, L361 (1993).

[24] T. A. Costi, J. Kroha, and P. Wölfle, Phys. Rev. B **53**, 1850 (1996). We thank the authors for providing us with the digital versions of their results.

[25] In the notation of Ref. 1, Eq. (58), this corresponds to writing $Y_1(\tau_i,\tau_f) = -\gamma(\tau_i)\Delta(\tau_i,\tau_f)$.

[26] E. Perepelitsky and B. S. Shastry, Ann. Phys. (NY) **338**, 283 (2013).

[27] J. Friedel, Can. J. Phys. **54**, 1190 (1956).

[28] J. S. Langer and V. Ambegaokar, Phys. Rev. **164**, 498 (1967).

[29] D. C. Langreth, Phys. Rev. **150**, 516 (1966).

[30] J. M. Luttinger and J. C. Ward, Phys. Rev. **118**, 1417 (1960).

[31] J. W. Rasul and A. C. Hewson, J. Phys. C: Solid State Phys. **17**, 3337 (1984).

[32] To recover Eq. (42), we may use Eq. (21) and the Fermi liquid assumption of $\mathrm{Im}\,\Sigma_{\mathrm{DM}}(0) = 0$ so that $\rho_{\mathcal{G}}(0) = \frac{1}{\pi}\frac{\Gamma_0(1-\frac{n_d}{2})^2}{\Gamma_0^2(1-\frac{n_d}{2})^2+[\epsilon_d+\mathrm{Re}\,\Sigma_{\mathrm{DM}}(0)]^2}$, and combine with Eq. (41).

[33] R. Žitko, D. Hansen, E. Perepelitsky, J. Mravlje, A. Georges, and B. S. Shastry, arXiv:1309.5284.

[34] X. Deng, J. Mravlje, R. Zitko, M. Ferrero, G. Kotliar, and A. Georges, Phys. Rev. Lett. **110**, 086401 (2013)